CANADIAN JOURNAL OF UROLOGY

Tech Science Press

Doi:10.32604/cju.2026.076790
ARTICLE

Study on automatic recognition of stone composition in intraoperative endoscopic images—a single center study

Daxun Luo,[#] Bixiao Wang,[#] Haifeng Song, Chaoyue Ji, Weiguo Hu, Bo Xiao, Boxing Su, Yubao Liu,[*] Jianxing Li,[*]

Department of Urology, Beijing Tsinghua Changgung Hospital, School of Clinical Medicine, Tsinghua University, Beijing, China

LUO D, WANG B, SONG H, JI C, HU W, XIAO B, SU B, LIU Y, LI J. Study on automatic recognition of stone composition in intraoperative endoscopic images—a single center study. *Can J Urol* 2026;33(3):623–634.

Objectives: *Urinary stone composition critically influences treatment selection and recurrence prevention, yet current intraoperative assessment remains imprecise. This study aims to achieve intraoperative prediction of stone composition by applying a deep convolutional neural network (CNN) to routinely captured endoscopic images.*

Methods: *We retrospectively studied endoscopic images from stone-breaking surgeries in Beijing Tsinghua Changgung Hospital during 2022-12–2024-12. Images were captured before and after laser lithotripsy. Based on postoperative infrared spectroscopy, stones were divided into five categories. In total, 1780 images (1167 from RIRS, 613 from PCNL) were included and split into training and testing sets at an 8:2 ratio. Using ResNet-50 as the base model, only endoscopic digital images and stone classification data were input for minimal-supervision learning. After training, the model accuracy for each stone category surpassed 95%. The model was then tested on 20% of RIRS and RIRS+PCNL images, with 3D PCA and Grad-cam for visual analysis.*

Results: *For the RIRS image test set: The precision was 93.8% for the calcium oxalate group (n = 147), 96.3% for the calcium oxalate mixed with a uric acid group (n = 30), 91.8% for the calcium oxalate mixed with carbonate apatite group (n = 106), 88.9% for the struvite mixed with calcium oxalate and carbonate apatite group (n = 16), and 100% for the stone free control group (n = 26) (Table 1). Total accuracy for CNN modeling is:94.16%, AUC:0.99, weighted F1-Score: 0.9353, weighted F1-score 95% CI: (0.9089, 0.9599), weighted Kappa: 0.9122, weighted Kappa 95% CI: (0.8523, 0.9569).For the RIRS+PCNL image test set: The precision was 94.9% for the calcium oxalate group (n = 195), 98.7% for the calcium oxalate mixed with a uric acid group (n = 80), 92.2% for the calcium oxalate mixed with carbonate apatite group (n = 111), 100% for the struvite mixed with calcium oxalate and carbonate apatite group (n = 29), and 93.8% for the stone free control group (n = 26) (Table 2).Total accuracy: 95.92%, AUC: 0.99, weighted F1-Score: 0.9508, weighted F1-score 95% CI: (0.9304, 0.9708) weighted Kappa: 0.9357, weighted Kappa 95% CI: (0.8907, 0.9678).The 3D PCA projection results are as follows: PC1: 0.2723 (27.23%), PC2: 0.1102 (11.02%), PC3: 0.0801 (8.01%), Cumulative: 46.26%.*

Conclusions: *This study shows deep CNNs can identify renal stone compositions from intraoperative endoscopic images, differentiating pure and mixed components. This analysis is an alternative to traditional methods and has the potential to improve treatment effectiveness.*

Key Words: deep convolutional neural network, urolithiasis composition prediction, endoscopic images, ResNet-50 model, diagnostic and therapeutic effectiveness

Introduction

Kidney stones are a common urological condition that significantly compromises patients' quality of life.[1,2] Their prevalence has been rising, largely attributable to lifestyle changes and environmental factors. With continuous technological advances, the therapeutic options for urinary stones have become increasingly

Received date 26 November 2025
Accepted for publication 30 January 2026
Published online 26 June 2026

[#]These authors contributed equally

*Corresponding Authors: Yubao Liu.
Email: lyba00854@btch.edu.cn; Jianxing Li.
Email: lijianxing2015@163.com

diverse: for stones smaller than 2 cm, flexible ureteroscopic lithotripsy (RIRS) is usually preferred, whereas percutaneous nephrolithotomy (PCNL) is favored for stones larger than 2 cm or staghorn calculi.[3,4] However, since different stone compositions necessitate varying treatment and prevention strategies, stone composition analysis is vital for personalized plans.[5] While infrared spectroscopy is the gold standard,[6–8] it is limited by cost and processing time. In China, each analysis typically costs from tens to several hundreds of RMB and requires 1–3 days for completion. Moreover, many hospitals rely on third-party laboratories due to lack of in-house testing capabilities, which may prolong analysis time and increase costs. Therefore, exploring a cutting-edge, simple, low-cost, and efficient method capable of observing stone structural characteristics is crucial.

Endoscopic image analysis, an emerging technique, can quickly and cost-effectively provide stone composition information and observe structural features, aiding in the selection of intraoperative lithotripsy parameters and postoperative prevention strategies.[9–11] It is easy to perform, promoting clinical application and enhancing stone analysis prevalence and accuracy, thus optimizing the diagnosis and treatment of urinary stones.

This study aims to develop a CNN model to identify stone compositions from intraoperative endoscopic images in urinary stone patients, exploring CNN's capability in this area and offering a novel, efficient analysis method for the clinic.

Data and Methods

Data collection

We retrospectively collected videos from 2022-12—2024-12 at Beijing Tsinghua Changgung Hospital. We collected surgical videos from 146 patients (Inclusion criteria for this study: 1. Preoperative diagnosis of urinary calculi; 2. Intraoperative video recording of the procedure; 3. Postoperative stone composition analysis. Exclusion criteria: 1. Poor-quality surgical video; 2. Absence of postoperative stone composition analysis.) From each video, 10–15 key frames were extracted for subsequent CNN training and validation. In total, 1780 images (1167 from RIRS, 613 from PCNL) were included. During frame extraction, we manually selected frames that exhibit distinct visual differences and deliberately minimized the inclusion of adjacent frames, enabling the CNN to better learn stone-specific features across the different classes. These videos recorded lithotripsy surgeries (RIRS and PCNL) performed by a single surgeon. The

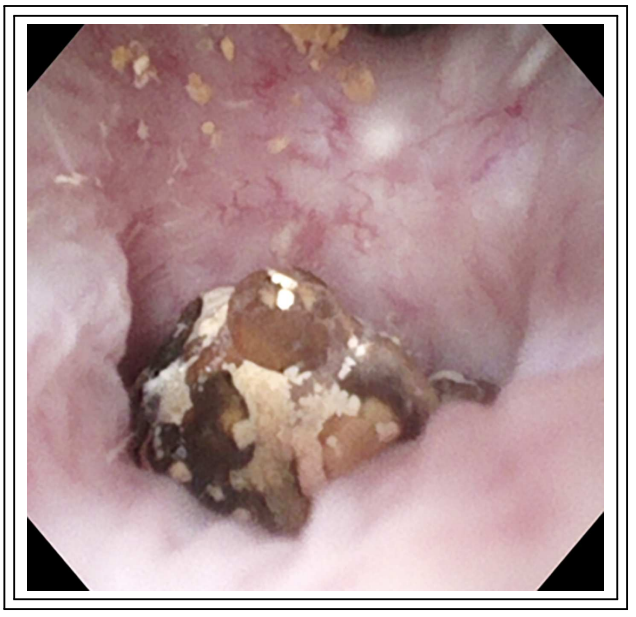

FIGURE 1. The stone (CaOx) surface before laser lithotripsy

eligible videos must include images of the stone surface and cross-section, with each segment recorded for over 3 s (Each image corresponds to a unique patient). Postoperatively, we used Potplayer software (https://potplayer.daum.net/) to capture frame-by-frame images of the stones before and after lithotripsy (Figures 1, 2). We excluded blurry or dust-interfered images. Finally, we classified and saved the images based on infrared spectroscopy results as preprocessed data.

As this study used retrospectively collected data, stone images were extracted as clear frames from archived surgical videos. In future prospective applications, the screenshot function integrated into most modern endoscopic systems can be used to capture suitable intraoperative images directly during the procedure, facilitating more efficient image collection in real-time clinical workflows.

RIRS and PCNL Equipment Imaging Systems:

Zebra RIRS: The electronic flexible ureteroscope weighs approximately 185 g. The insertion shaft has a distal outer diameter of F7.4 (maximum F8.6) and a single working channel of F3.6. The distal tip offers 1:1 coaxial deflection with a minimum bend radius of ~8 mm and maintains bidirectional angulation >270° whether unloaded or loaded with a 200 μm holmium laser fiber. A distal CMOS sensor provides high-definition electronic imaging at 160 000 pixels; the imaging console can be connected to external monitors.

FIGURE 2. The relatively intact cross-sectional image of the stone (CaOx) after laser lithotripsy

Storz PCNL: The imaging platform delivers both 2-D and 3-D full-HD video (resolution $\geq 1920 \times 1080$). It incorporates an integrated 2-D full-HD capture and recording subsystem that supports unlimited, synchronous dual-channel 1080p acquisition. Video outputs include dual DVI or HDMI ports and a 3G-SDI interface, all providing full-HD 1080p signals.

All endoscopic still frames were exported by the imaging console in JPEG format at a resolution of 1920×1080 pixels. The images are 24-bit true-color and encoded in standard RGB; no CMYK, monochrome, or additional spectral channels were used. This configuration reflects the default output of both the Zebra RIRS and Storz PCNL systems, ensuring that the visual inputs processed by the CNN are identical to those displayed to the surgeon in real time.

Data preparation

To enhance algorithm accuracy, data pretreatment is essential.

1) Data grouping: Based on postoperative Fourier Transform Infrared Spectroscopy (FTIR), the data is divided into four groups(Calcium Oxalate; Calcium Oxalate + Uric Acid; Calcium Oxalate + Calcium Apatite; Struvite+ Carbonate Apatite mixed stones), with the addition of a stone free control group. The stone-free control group was defined as endoscopic images displaying normal renal tissue without any visible stones. This category was included to train the model to distinguish normal anatomy from stone-containing images, thereby improving overall classification accuracy and reducing false positive predictions. Mixed stones are defined as those composed of two or more distinct mineral components, based on postoperative FTIR results. However, the exact compositional percentage of each component was not specified or used for classification in this study.

2) Rebalancing and data augmentation: To address category imbalance, we applied data augmentation techniques such as random cropping, random occlusion, and used a weighted loss function during model training. These approaches serve to synthetically expand the dataset for minority classes and adjust model training to prevent dominance by overrepresented categories.

Model construction

CNN, first put forward by Yann Lecun in 1989, is now a mainstay in neural network research.[12] Given their use of convolutional kernels to extract image features, CNNs excel at handling image data. Among various training models, ResNet is one of the most widely used CNN structures, which is optimized via residual learning and shortcut connections.[13,14] In this study, stone composition analysis is treated as an image classification problem. After trying many deep visual models, ResNet-50 is chosen as the base, with a custom expert network added to fit the task. Compared with traditional models, its 50-layer depth can extract more features for accurate stone composition analysis. A multi-layer fully connected neural network is added to output stone categories. The model is trained with endoscopic images and stone classification data for minimal supervision learning. The whole CNN training structure is shown in Figure 3.

Model evaluation and data analysis

This study applies Python 3.13.11 for data analysis and CNN model construction. The dataset is split into training (80%) and testing (20%) sets randomly. After training on the training set, the testing set (unseen by the model) is used to check generalization. The model's training accuracy for each stone category is over 95%. For stone composition analysis, the evaluation metrics are accuracy, recall, specificity, F1-score, and Kappa value (Tables 1 and 2). Model performance is assessed via confusion matrices (Figures 4 and 5). ROC curves (Figures 6 and 7) are also used to evaluate the model's performance. Images from both RIRS and PCNL procedures were used jointly during training to improve model robustness. For evaluation, we first tested the model on a test set

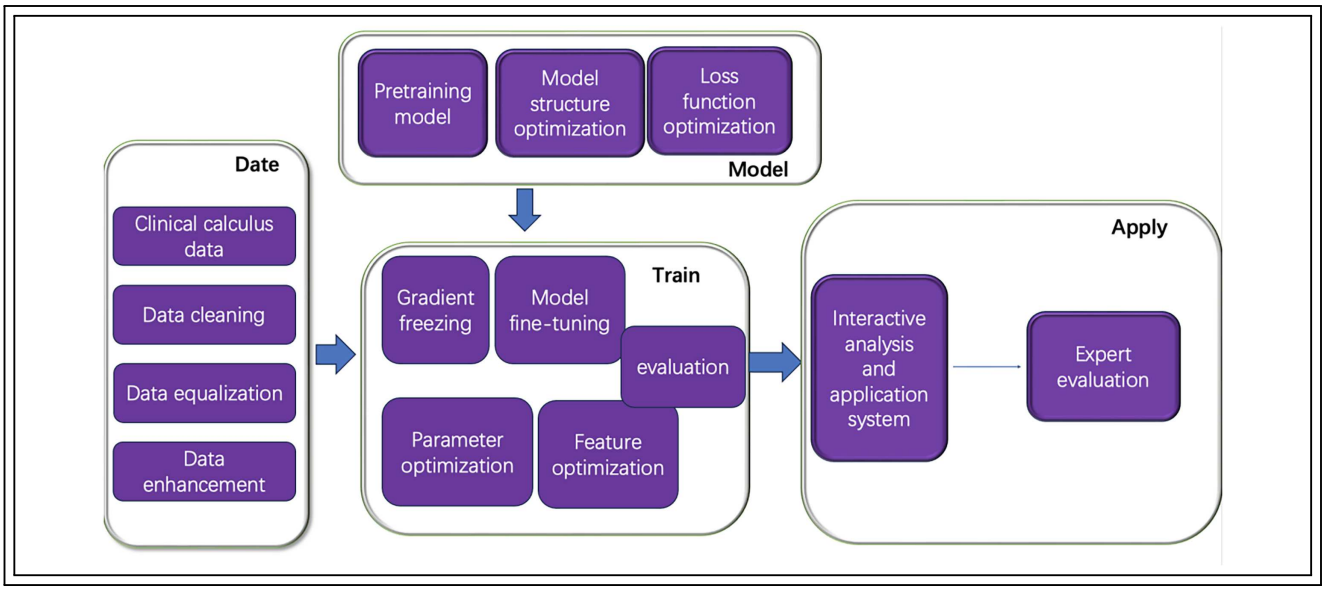

FIGURE 3. Flowchart of the present study

TABLE 1. **Results of the RIRS test set**

Stone Composition	Precision (%)	Recall (%)	Specificity (%)	F1-Score	AUC (95%CI)
Calcium oxalate stones	93.8%	93.2%	94.9%	0.9352	0.99 (0.9790, 0.9959)
Calcium oxalate and uric acid stones	96.3%	86.7%	99.7%	0.9123	0.98 (0.9549, 0.9990)
Calcium oxalate and carbonate apatite stones	91.8%	95.3%	95.9%	0.9352	0.99 (0.9683, 0.9963)
Struvite, calcium oxalate, and carbonate apatite mixed stones	88.9%	100%	99.4%	0.9412	1.00 (0.9692, 1.0000)
Stone free control group	100%	92.3%	100%	0.9600	1.00 (0.9940, 1.0000)

Note. **AUC:** Area Under the Curve.

consisting solely of RIRS images to assess performance in a uniform context, followed by testing on a mixed RIRS+PCNL test set to evaluate generalization across different endoscopic modalities. 3D PCA plots (Figure 8) are drawn for visual analysis of RIRS and RIRS+PCNL images, checking the consistency of their image features. This retrospective study was approved by the Institutional Review Board of Beijing Tsinghua Changgung Hospital (Approval No. 24442-0-02), which waived the requirement for informed consent.

Results

For the RIRS image test set: The precision was 93.8% for the calcium oxalate group (n = 147), 96.3% for the calcium oxalate mixed with a uric acid group (n = 30), 91.8% for the calcium oxalate mixed with carbonate apatite group (n = 106), 88.9% for the struvite mixed with calcium oxalate and carbonate apatite group (n = 16), and 100% for the stone free control group (n = 26) (Table 1). Total accuracy for CNN modeling is: 94.16%, AUC:0.99, weighted F1-Score: 0.9353, weighted F1-score 95% CI: (0.9089, 0.9599), weighted Kappa: 0.9122, weighted Kappa 95% CI: (0.8523, 0.9569).

For the RIRS+PCNL image test set: The precision was 94.9% for the calcium oxalate group (n = 195), 98.7% for the calcium oxalate mixed with a uric acid group (n = 80), 92.2% for the calcium oxalate mixed with carbonate apatite group (n = 111), 100% for

TABLE 2. **Results of the RIRS + PCNL test set**

Stone Composition	Precision (%)	Recall (%)	Specificity (%)	F1-Score	AUC (95%CI)
Calcium oxalate stones	94.9%	94.9%	96%	0.9490	0.99 (0.9810, 0.9958)
Calcium oxalate and uric acid stones	98.7%	93.8%	99.7%	0.9620	0.99 (0.9835, 0.9996)
Calcium oxalate and carbonate apatite stones	92.2%	95.5%	97.3%	0.9386	0.99 (0.9792, 0.9977)
Struvite, calcium oxalate, and carbonate apatite mixed stones	100%	92.6%	97.7%	0.9677	1.00 (0.9280, 1.0000)
Stone free control group	93.8%	100%	99.5%	0.9615	1.00 (0.9961, 1.0000)

Note. **AUC:** Area Under the Curve.

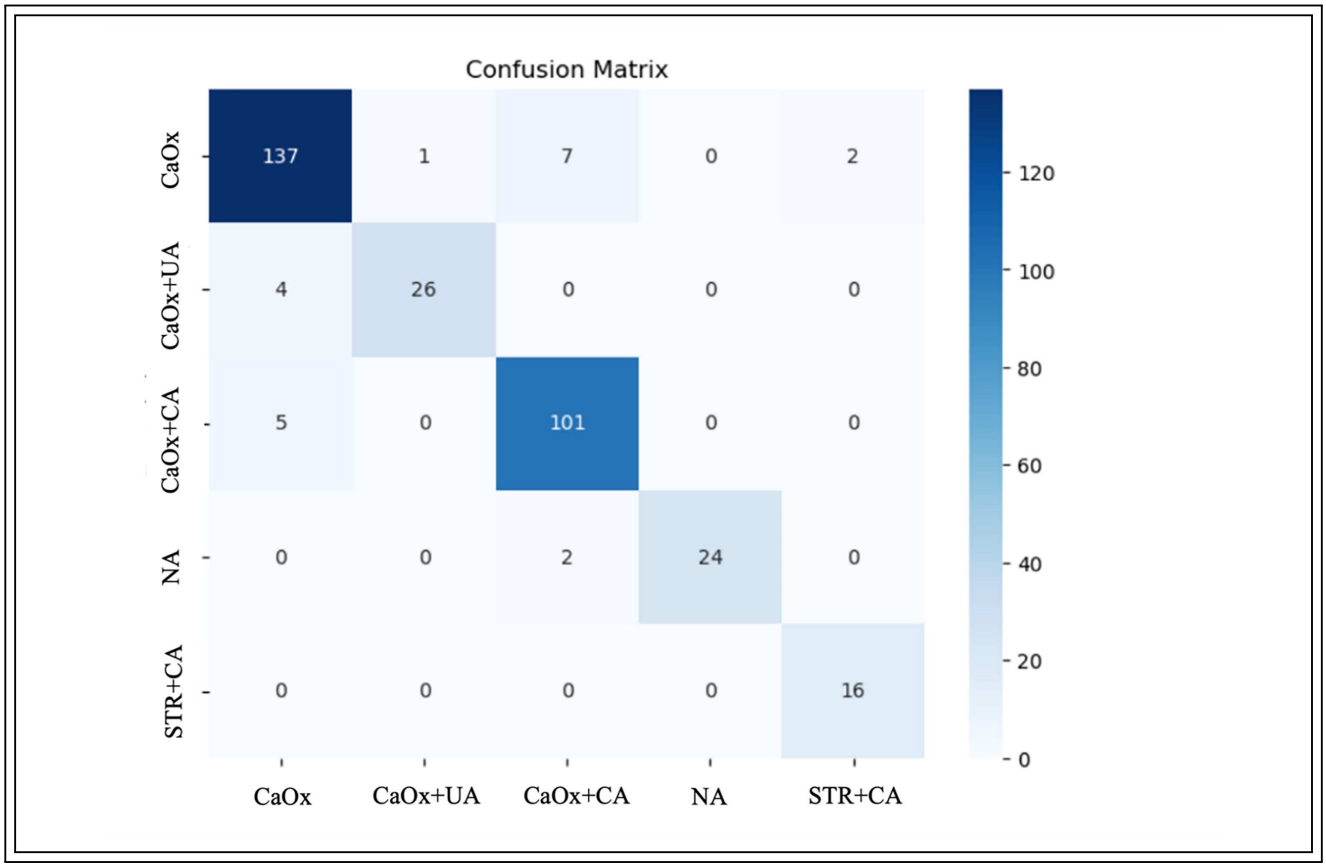

FIGURE 4. Confusion matrix of RIRS test set. CaOx: Calcium Oxalate**; CaOx+UA:** Calcium Oxalate + Uric Acid**; CaOx+CA:** Calcium Oxalate + Calcium Apatite**;** NA: Stone free control group; **STR+CA:** Struvite+Calcium Oxalate, and Carbonate Apatite mixed stones

the struvite mixed with calcium oxalate and carbonate apatite group (n = 29), and 93.8% for the stone free control group (n = 26) (Table 2). Total accuracy: 95.92%, AUC: 0.99, weighted F1-Score: 0.9508, weighted F1-score 95% CI: (0.9304, 0.9708) weighted Kappa: 0.9357, weighted Kappa 95% CI: (0.8907, 0.9678).

The 3D PCA projection results are as follows: PC1: 0.2723 (27.23%), PC2: 0.1102 (11.02%), PC3: 0.0801 (8.01%), Cumulative: 46.26%.

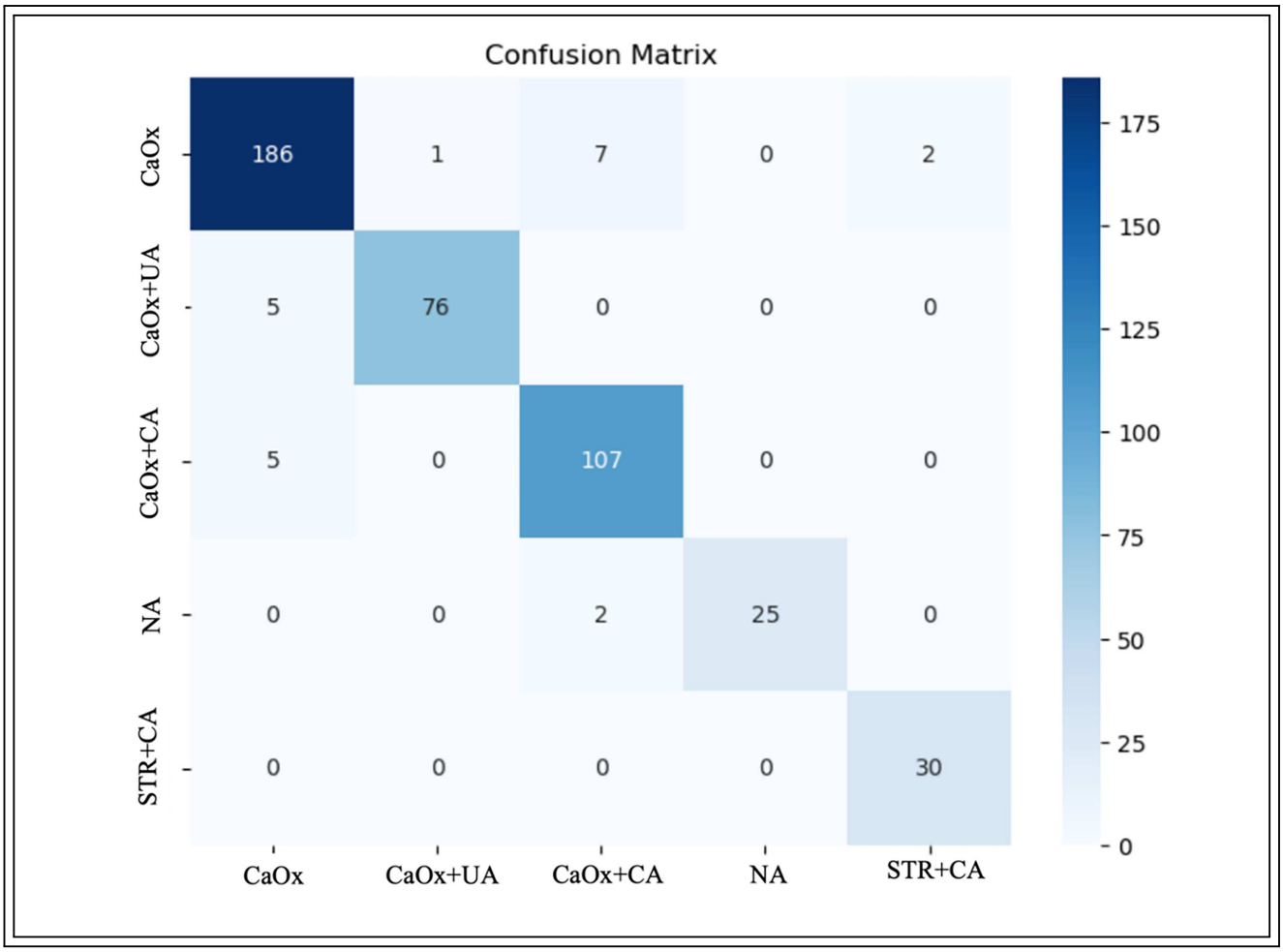

FIGURE 5. Confusion Matrix of RIRS+PCNL Test Set. **CaOx:** Calcium Oxalate**; CaOx+UA:** Calcium Oxalate + Uric Acid**; CaOx+CA:** Calcium Oxalate + Calcium Apatite**; NA:** Stone free control group**; STR+CA:** Struvite+Calcium Oxalate, and Carbonate Apatite mixed stones

Discussion

In the past, due to technological limitations, doctors could only determine stone composition postoperatively through test kits or infrared spectroscopy, which lacked preoperative or intraoperative certainty. Although experienced clinicians might roughly predict stone composition based on the typical appearance of intraoperative stone images, the SEGUR study[15] revealed that results from direct intraoperative image observation by experience are unreliable. The study had 32 doctors from 9 countries watch videos of endoscopic stone findings and predict stone composition, achieving an overall accuracy of only 39% (250/640). In contrast, the CNN model for two surgical methods in our study reached accuracies of 94.16% and 95.92%, indicating that the trained CNN model has a higher accuracy in identifying stone composition than experienced clinicians.

Although intraoperative visual estimation of stone composition remains unreliable, the idea of inferring composition from stone appearance has opened a new avenue for artificial-intelligence-based recognition. Huang's team[16] used preoperative dual-energy CT (DECT) to predict stone composition, achieving an AUC of 0.83. While DECT offers promising predictive capability, especially for non-mixed stones, it has limitations in identifying mixed compositions and non-uric acid stones. Moreover, the cost and accessibility of DECT remain barriers to its widespread use. Therefore, our approach aims to offer a supplementary solution by utilizing intraoperative endoscopic

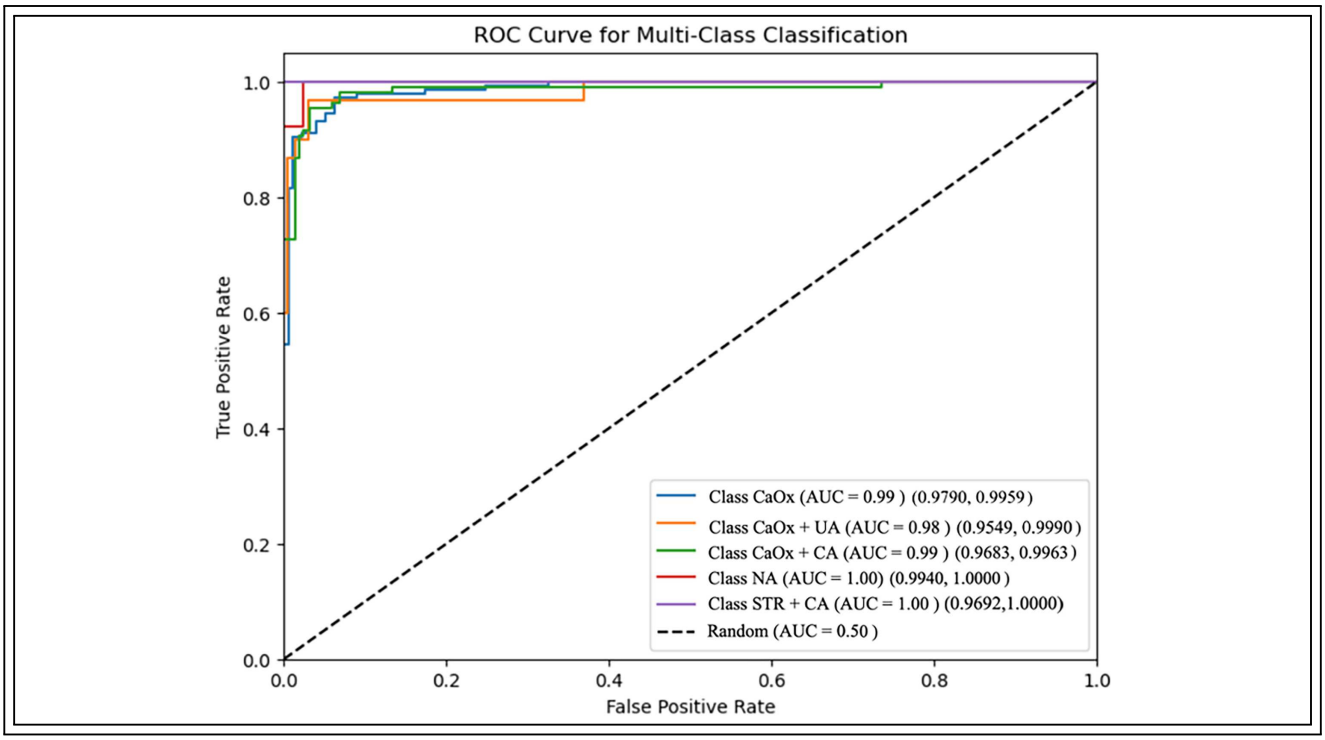

FIGURE 6. ROC Curve of RIRS Test Set. **CaOx:** Calcium Oxalate**; CaOx+UA:** Calcium Oxalate + Uric Acid**; CaOx+CA:** Calcium Oxalate + Calcium Apatite**; NA:** Stone free control group**; STR+CA:** Struvite+Calcium Oxalate, and Carbonate Apatite mixed stones

images, enabling physicians to refine and clarify diagnoses during surgery, and enhancing their confidence in performing surgical procedures. In our study, the CNN model achieved AUC values of 0.99 (Figures 6 and 7), indicating not only good discrimination but also the ability to identify uric acid stones and predict specific components of non-uric acid stones. In recent years, Black's team[17] recently used deep-learning on *ex-vivo* stone photos and reached 75–95% accuracy and 85% recall, showing the promise of AI for compositional analysis. We go one step further: we train and test on intraoperative images, overcoming the small datasets, variable surgical scenes, and limited clinical relevance of *ex-vivo* photography.

In this study, we used a CNN model to predict urinary stone composition from intraoperative endoscopic images and achieved preliminary results. Our data selection approach is akin to those of Oh and Estrade's teams,[18,19] who harnessed intraoperative RIRS stone images for deep-learning-based composition identification. The former attained 81.8% accuracy in differentiating calcium-containing from non-calcium-containing stones, while the latter broadened the identifiable composition scope. Notably, Kyung's team[20] didn't incorporate intraoperative cross-sectional urinary stone images into their research. Given that mixed composition, stones may have differing surface and core components,[21] our study enhances the methodology by boosting the data volume, adding PCNL images for training, expanding the stone classification groups, refining the data results (including Kappa, 95% CI, etc.), and incorporating both pre and post lithotripsy cross-sectional images into the training model. Analysis of our study's results reveals that CNN offers significant advantages in feature extraction and classification. Moreover, the inclusion of PCNL images, in addition to RIRS images during model training, ensures greater adaptability to diverse clinical equipment.

In model selection, Kim's team[22] achieved significant results using the Xception model, which has fewer parameters and a smaller computational load than ResNet-50, potentially making it less effective for complex image features. Zhu and Black's teams[17,18] used the ResNet-101 model, achieving an overall recall of 99%. We chose ResNet-50 (50 layers) over deeper models to avoid overfitting given our current data volume and complexity, ensuring faster operation and better performance. Leng's team[23] used the

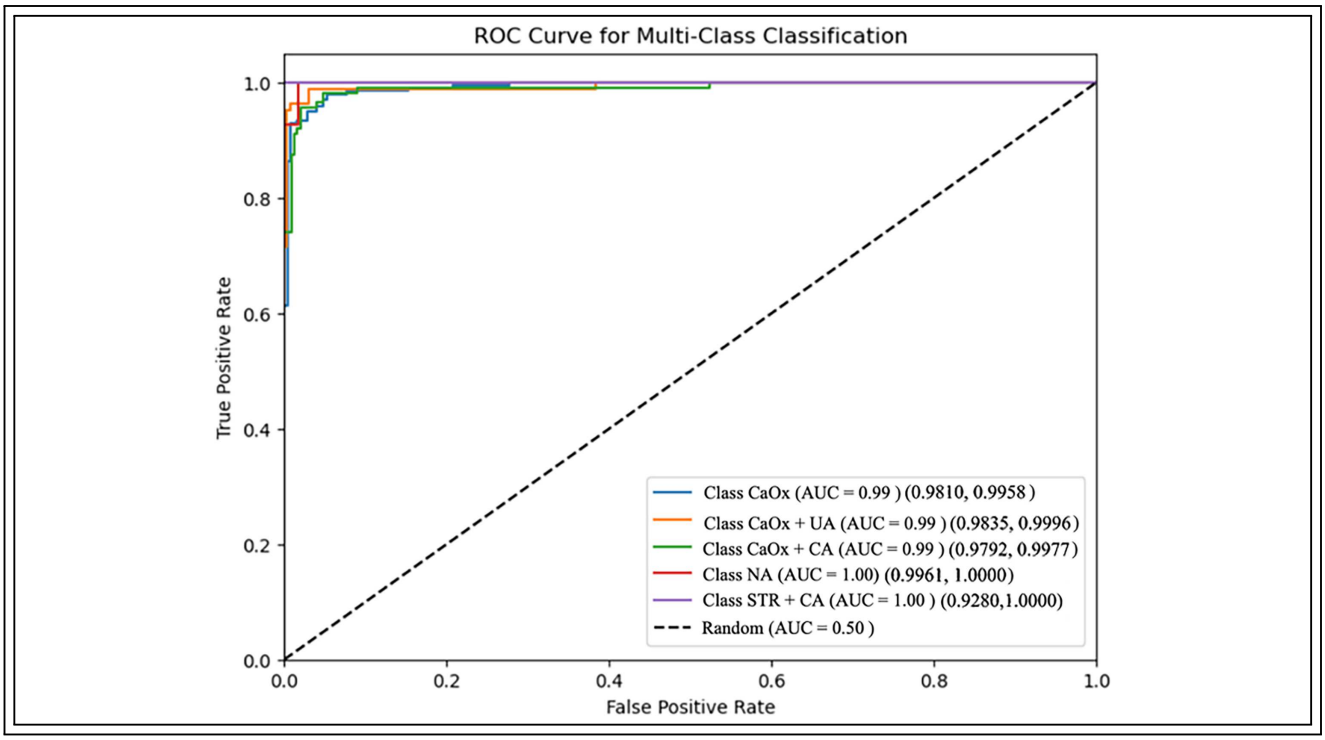

FIGURE 7. ROC Curve of RIRS+PCNL Test Set. **CaOx:** Calcium Oxalate**; CaOx+UA:** Calcium Oxalate + Uric Acid**; CaOx+CA:** Calcium Oxalate + Calcium Apatite**; NA:** Stone free control group**; STR+CA:** Struvite+Calcium Oxalate, and Carbonate Apatite mixed stones

SAM model, which had a lower overall accuracy (60%) compared to our study, possibly because SAM is better suited for segmentation tasks rather than image classification, where ResNet excels. Estrade's team[19] used the same model as us but focused mainly on calcium oxalate and its subtypes for stone classification, whereas our study includes a broader range of components such as struvite and carbonate apatite. Additionally, ResNet allows for transfer learning on pre-trained models, saving training time and computational resources. Our study gradually enriches the dataset, and as the data volume grows, deep learning models will be better supported and overfitting avoided.

In terms of learning method selection, Leng's team[23] applied a machine learning model to automatically identify renal stone composition from endoscopic videos. They extracted frames and manually outlined the stones for model training, achieving a classification accuracy of 62%. The low accuracy may be due to the model's limitation in learning from manually outlined regions of interest (ROIs). In contrast, our study minimally preprocessed and classified intraoperative stone images before CNN model training, allowing the model to learn directly from the image pixels through convolution, achieving good accuracy with less human interventions. Finally, we conducted an interpretability analysis of Grad-CAM (Figure 9).[24] According to the information in the figure, we can find that the CNN model pays more attention to the stones in the pictures during the training process. Therefore, it visually verifies that CNN can accurately locate and identify the stone components, providing a visual basis for its high accuracy rate.

During surgical procedures, different stone compositions require different laser lithotripsy parameters.[25] Although Eren's team[26] found that high-power lithotripsy can reduce surgical and hospitalization time, it also poses risks such as thermal damage to surrounding tissues, stone displacement, and higher costs. Our study aligns with Lena's concept[27] of real-time data analysis for surgical decision-making. Prolonged surgeries (over 2 h) can increase postoperative complications,[28–30] while prior studies have demonstrated that stone hardness influences laser efficiency, incorporating real-time composition feedback during surgery may further assist surgeons in tailoring lithotripsy settings, especially when preoperative predictions

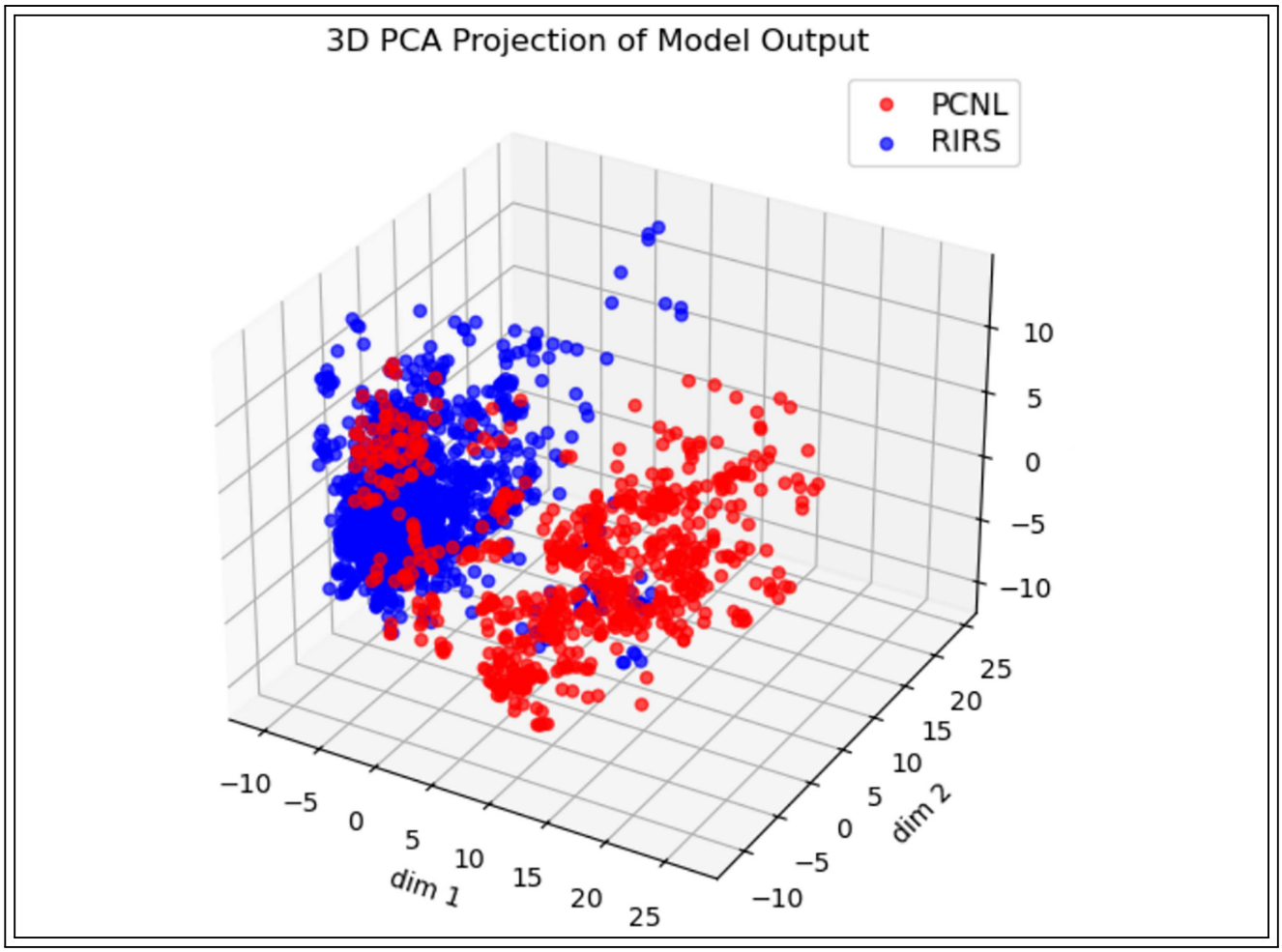

FIGURE 8. 3D PCA Projection Plot. PCA: Principal Component Analysis**; PCNL:** Percutaneous Nephrolithotomy**; RIRS:** Retrograde Intrarenal Surgery

are inconclusive. This may help reduce operative time, lower the risk of complications, and enhance procedural safety and effectiveness.[31] Moreover, accurate intraoperative stone identification allows for immediate postoperative preventive measures, such as a low purine diet for uric acid stones, urine alkalization for calcium oxalate stones, and anti-infective treatment for struvite stones, providing clear directions for preventing recurrence.

It is important to note that this study did not perform real-time analysis in the strictest sense, as image acquisition was conducted retrospectively using extracted video frames. In future clinical implementation, however, intraoperative image capture could be achieved directly using the screenshot function of the surgical endoscope. With proper integration into endoscopic platforms or surgical software, this workflow may enable rapid intraoperative prediction to assist clinical decision-making. Rapid analysis within a short time frame can guide the setting of lithotripsy parameters, reduce stone composition analysis time, and enhance surgical accuracy and efficiency. Additionally, it can compensate for postoperative sampling errors in infrared spectroscopy, with low analysis costs for widespread use in primary hospitals. Furthermore, it provides comprehensive stone structure information for long term etiological research.

While we've achieved certain results, limitations remain. Calcium oxalate subtype differentiation is crucial for determining appropriate laser lithotripsy settings, because calcium oxalate monohydrate (COM) stones are denser and more resistant than calcium oxalate dihydrate (COD) stones. Due to limited annotated data, this study did not distinguish

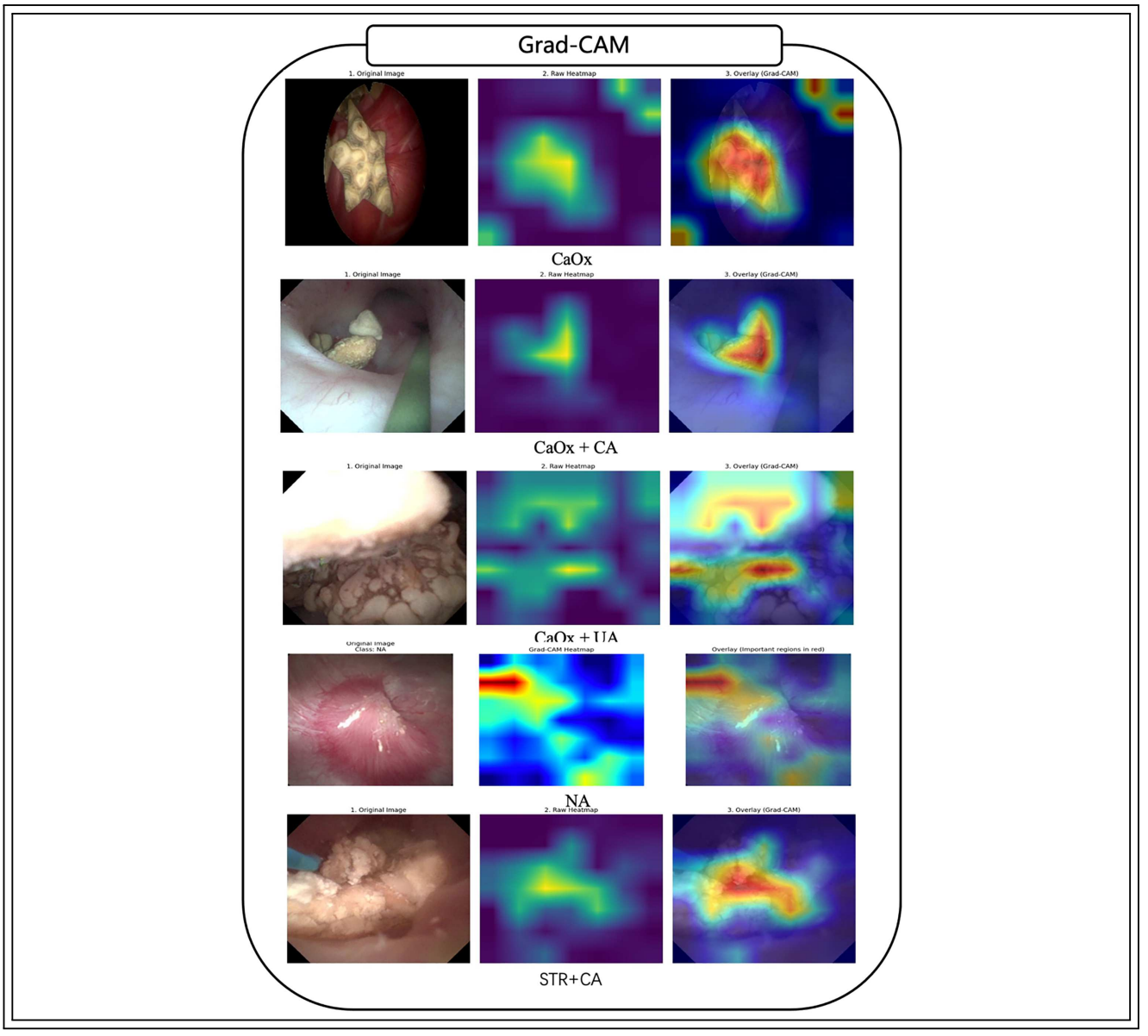

FIGURE 9. Grad-CAM. CaOx: Calcium Oxalate**; CaOx+UA:** Calcium Oxalate + Uric Acid**; CaOx+CA:** Calcium Oxalate + Calcium Apatite**; NA:** Stone free control group**; STR+CA:** Struvite+Calcium Oxalate, and Carbonate Apatite mixed stones

between these subtypes. As additional samples become available, we plan to incorporate subtype classification to further support personalized intraoperative laser parameter selection. The grouping of stone components in this study was limited by the availability and distribution of clinical data. Notably, although uric acid stones were historically more common in our dataset, a temporal shift in patient characteristics during the data collection period led to a lower representation. As a result, we could not include a pure uric acid category in the final model. In addition, the 3D-PCA plot should be noted as follows: it accounts for only 46.26% of the total variance, indicating that the data are intrinsically high-dimensional and the scatter plot can display merely a partial structure. Nevertheless, the RIRS and PCNL point clouds overlap at the centre yet separate along the principal axes, in other words, although images from RIRS and PCNL can be distinguished, the endoscopic images obtained are

generally consistent; the intracavitary pictures from the two systems are also mutually complementary for stone identification. In future studies, we aim to refine and expand the classification scheme using larger and more balanced datasets aligned with standardized definitions. Due to technical constraints and sample size limitations, the image-based method presented in this study cannot determine the precise percentage composition of different components within mixed stones, unlike FTIR spectroscopy. Further research will explore methods to estimate compositional ratios, potentially incorporating multi-modal data sources or hybrid imaging approaches. Lastly, the model was trained on images from Zebra RIRS and Storz PCNL devices, and we will incorporate more brands to enhance generalizability across different endoscopic equipment.

Conclusion

This study shows deep CNNs can identify renal stone compositions from intraoperative endoscopic images, differentiating pure and mixed components. This analysis is an alternative to traditional methods and has the potential to improve treatment effectiveness.

Acknowledgement

We extend our heartfelt gratitude to all colleagues who supported and assisted this study. We thank the medical staff involved in data collection and annotation, as well as our laboratory teammates for their dedicated help in algorithm implementation and computational resources. Special appreciation goes to our mentors and peer experts for their invaluable suggestions and selfless guidance during topic selection, experimental design, and manuscript preparation. The successful completion of this work would not have been possible without the concerted efforts of the entire team and the generous support of all contributors.

Funding Statement

The authors received no specific funding for this study.

Author Contributions

All authors contributed to the study conception and design. The experiments were designed by Bixiao Wang, Yubao Liu, and Jianxing Li. Data collection and analysis were performed by Haifeng Song, Chaoyue Ji, Weiguo Hu, Bo Xiao, and Boxing Su. The first draft of the manuscript was written by Daxun Luo, and all authors commented on previous versions of the manuscript. The corresponding authors, Yubao Liu and Jianxing Li, supervised the study throughout. All authors reviewed and approved the final version of the manuscript.

Availability of Data and Materials

No datasets were generated or analysed during the current study.

Ethics Approval

This retrospective study was approved by the Institutional Review Board of Beijing Tsinghua Changgung Hospital (Approval No. 24442-0-02), which waived the requirement for informed consent.

Conflict of Interest

The authors declare no conflicts of interest.

References

1. Zeng G, Mai Z, Xia S et al. Prevalence of kidney stones in China: an ultrasonography based cross-sectional study. *BJU Int* 2017;120(1):109–116. doi:10.1111/bju.13828.
2. Bargagli M, Scoglio M, Howles SA, Fuster DG. Kidney stone disease: Risk factors, pathophysiology and management. *Nat Rev Nephrol* 2025;21(11):794–808. doi:10.1038/s41581-025-00990-x.
3. Soderberg L, Ergun O, Ding M et al. Percutaneous nephrolithotomy versus retrograde intrarenal surgery for treatment of renal stones in adults. *Cochrane Database Syst Rev* 2023;11(11):CD013445. doi:10.1002/14651858.CD013445.pub2.
4. Ying Z, Ming S, Yang R et al. Comparison of safety and efficacy of negative pressure aspiration assisted retrograde intrarenal surgery and traditional percutaneous nephrolithotomy in the treatment of upper urinary tract stones larger than 2 Cm: A systematic review and meta-analysis. *Int J Surg* 2025;111(5):3613–3628. doi:10.1097/JS9.0000000000002363.

5. Williams JC, Gambaro G, Rodgers A et al. Urine and stone analysis for the investigation of the renal stone former: A consensus conference. *Urolithiasis* 2021;49(1):1–16. doi:10.1007/s00240-020-01217-3.
6. Basiri A, Taheri M, Taheri F. What is the state of the stone analysis techniques in urolithiasis? *Urol J* 2012;9(2):445–454.
7. Singh I. Renal geology (quantitative renal stone analysis) by 'Fourier transform infrared spectroscopy'. *Int Urol Nephrol* 2008;40(3):595–602. doi:10.1007/s11255-007-9327-2.
8. Daudon M, Haymann JP, Estrade V, Meria P, Almeras C. 2022 Recommendations of the AFU lithiasis committee: epidemiology, stone analysis and composition. *Prog Urol* 2023;33(14):737–765. doi:10.1016/j.purol.2023.08.013.
9. Teichman JM, Vassar GJ, Glickman RD. Holmium: yttrium-aluminum-garnet lithotripsy efficiency varies with stone composition. *Urology* 1998;52(3):392–397. doi:10.1016/s0090-4295(98)00239-8.
10. Panthier F, Ventimiglia E, Berthe L et al. How much energy do we need to ablate 1 mm(3) of stone during Ho: YAG laser lithotripsy? An *in vitro* study. *World J Urol* 2020;38(11):2945–2953. doi:10.1007/s00345-020-03091-5.
11. Wang C, Liang H, Chen H et al. Clinical validation of an AI-assisted system for real-time kidney stone detection during flexible ureteroscopic surgery. *npj Digit Med* 2025;8(1):728. doi:10.1038/s41746-025-02109-9.
12. Duponchel L, Rocha de Oliveira R, Motto-Ros V. Large language models (such as ChatGPT) as tools for machine learning-based data insights in analytical chemistry. *Anal Chem* 2025;97(13):6956–6961. doi:10.1021/acs.analchem.4c05046.
13. Srivastava R, Kumar N, Sandhan T. Binary classification of laryngeal images utilising ResNet-50 CNN architecture. *Indian J Otolaryngol Head Neck Surg* 2025;77(2):644–651. doi:10.1007/s12070-024-05202-9.
14. Seng H, Argha A, Liaw ST, Celler BG, Marks GB. Machine and deep learning for tuberculosis detection on chest X-rays: Systematic literature review. *J Med Internet Res* 2023;25(3):e43154. doi:10.2196/43154.
15. Sampogna G, Basic D, Geavlete P et al. Endoscopic identification of urinary stone composition: A study of South Eastern Group for Urolithiasis Research (SEGUR 2). *Actas Urológicas Españolas Engl Ed* 2021;45(2):154–159. doi:10.1016/j.acuroe.2021.01.004.
16. Huang J, Hou J, Yang W et al. Automatic kidney stone composition analysis method based on dual-energyCT. *Curr Med Imag Former Curr Med Imag Rev* 2023;20:e080923220827. doi:10.2174/1573405620666230908111745.
17. Black KM, Law H, Aldoukhi A, Deng J, Ghani KR. Deep learning computer vision algorithm for detecting kidney stone composition. *BJU Int* 2020;125(6):920–924. doi:10.1111/bju.15035.
18. Zhu G, Li C, Guo Y et al. Predicting stone composition via machine-learning models trained on intra-operative endoscopic digital images. *BMC Urol* 2024;24(1):5. doi:10.1186/s12894-023-01396-2.
19. Estrade V, Daudon M, Richard E et al. Towards automatic recognition of pure and mixed stones using intra-operative endoscopic digital images. *BJU Int* 2022;129(2):234–242. doi:10.1111/bju.15515.
20. Oh KT, Jun DY, Choi JY, Jung DC, Lee JY. Predicting urinary stone composition in single-use flexible ureteroscopic images with a convolutional neural network. *Medicina* 2023;59(8):1400. doi:10.3390/medicina59081400.
21. Daudon M, Jungers P. Clinical value of crystalluria and quantitative morphoconstitutional analysis of urinary calculi. *Nephron Physiol* 2004;98(2):31–36. doi:10.1159/000080261.
22. Kim US, Kwon HS, Yang W et al. Prediction of the composition of urinary stones using deep learning. *Investig Clin Urol* 2022;63(4):441–447. doi:10.4111/icu.20220062.
23. Leng J, Liu J, Cheng G et al. Development of UroSAM: a machine learning model to automatically identify kidney stone composition from endoscopic video. *J Endourol* 2024;38(8):748–754. doi:10.1089/end.2023.0740.
24. Fayyaz AM, Abdulkadir SJ, Talpur N, Al-Selwi SM, Hassan SU, Sumiea EH. Grad-CAM (Gradient-weighted Class Activation Mapping): a systematic literature review. *Comput Biol Med* 2025;198(Pt B):111200. doi:10.1016/j.compbiomed.2025.111200.
25. Ulvik Ø, Æsøy MS, Juliebø-Jones P, Gjengstø P, Beisland C. Thulium fibre laser versus holmium: YAG for ureteroscopic lithotripsy: Outcomes from a prospective randomised clinical trial. *Eur Urol* 2022;82(1):73–79. doi:10.1016/j.eururo.2022.02.027.
26. Erol E, Ecer G, Kiremit MC et al. Multicentric evaluation of high and low power lasers on RIRS success using propensity score analysis. *Urolithiasis* 2024;52(1):32. doi:10.1007/s00240-024-01535-w.
27. Maier-Hein L, Vedula SS, Speidel S et al. Surgical data science for next-generation interventions. *Nat Biomed Eng* 2017;1(9):691–696. doi:10.1038/s41551-017-0132-7.
28. Ao P, Shu L, Zhuo D et al. Risk factors associated with systemic inflammatory response syndrome after flexible ueteroscopic lithotripsy based on enhanced recovery after surgery. *Zhonghua Yi Xue Za Zhi* 2019;99(10):758–763. doi:10.3760/cma.j.issn.0376-2491.2019.10.010.
29. Ye S, Wang W, Yu Z, Luo J. Risk factors for systemic inflammatory response syndrome after endoscopic lithotripsy for upper urinary calculi. *BMC Urol* 2023;23(1):59. doi:10.1186/s12894-023-01230-9.
30. Tan D, Wu F, Huo W. Clinical characteristics and risk factors of systemic inflammatory response syndrome after flexible ureteroscopic lithotripsy. *Arch Esp Urol* 2022;75(7):618–623. doi:10.56434/j.arch.esp.urol.20227507.89.
31. Liang H, Liang L, Yu Y et al. Thermal effect of holmium laser during ureteroscopic lithotripsy. *BMC Urol* 2020;20(1):69. doi:10.1186/s12894-020-00639-w.